Electron energy distributions in electron cyclotron resonance discharges for materials processing

Yilin Weng and Mark J. Kushner[a]
Department of Electrical and Computer Engineering, University of Illinois, 1406 W. Green Street, Urbana, Illinois 61801

Electron cyclotron resonance (ECR) reactors are now being investigated for use in the plasma processing of semiconductors. The attractive feature of ECR excitation is that high plasma densities (10^{10}–10^{12} cm^{-3}) can be obtained at low pressures (0.1–a few mTorr). In this paper, we present results from a computer simulation of the electron kinetics in ECR reactors. The model is a multidimensional Monte Carlo simulation coupled with a fluid simulation with which the electron energy distribution (EED) may be calculated. We find that the electron temperature ($T_e = \frac{2}{3}\langle\epsilon\rangle$) in Ar plasmas (0.1–10 mTorr, 100s W) is 10–20 eV in the ECR zone, falling to a few to 5 eV downstream of the ECR zone, in general agreement with experiments. The EED can be described as being multitemperature with a low energy component (5–10 eV) and a high energy tail extending to many 10s to 100s eV. Predicted ambipolar potentials are 10–30 V, increasing with decreasing pressure and increasing power deposition.

I. INTRODUCTION

Reactive ion etching (RIE) using radio frequency (rf) diode discharges is currently the standard process for etching semiconductors in the fabrication of microelectronic devices.[1] Although these reactors are industry standards, alternate reactor configurations are concurrently being investigated. The goals of these efforts are to obtain more anisotropic etching and more control over depositions with higher degrees of uniformity over larger areas. These attributes can be obtained by operating at high power deposition and low gas pressures. Electron cyclotron resonance (ECR) discharges are being studied as a means to meet these goals.[2–15] ECR discharges, as used in the etching of semiconductors, typically operate at gas pressures of 0.1 mTorr to a few mTorr, plasma densities of 10^{10}–10^{12} cm^{-3} and electron temperatures of a few to 10s eV in the source region. The reactors are typically 10–20 cm in diameter in the resonance region, expanding to a larger diameter in a downstream chamber where the substrate is usually located. [see Fig. 1(a)]. The resonant microwave frequency, v_r, is most commonly 2.45 Ghz corresponding to ECR occurring at a magnetic field of $B = 875$ G.

ECR reactors, as materials processing tools, are commonly thought of as being remote devices. That is, the plasma is sustained upstream from the wafer. In this view, excitation and ionization dominantly occur in the resonance zone with products flowing to the wafer downstream. The remote location of the substrate, though, does not preclude its being bombarded by energetic particles. Spectroscopic and energy analyzer measurements of ion temperatures and energies in ECR reactors have shown that the ion flux incident onto the substrate has energies of a few to 10s eV, and temperatures of many tenths of an eV.[9,10,14,15] The maximum ion energies are commensurate with the ambipolar generated plasma potential.

At a gas pressure of 1 mTorr, the mean free path for electron collisions is many to 10s cm, and the electron collision frequency is approximately $v_c = 5 \times 10^6$ s^{-1}. The plasma is therefore magnetized ($v_c/v_r = 0.002$) and electrons have a high mobility parallel to the magnetic field. This allows electron energy transport from the ECR zone downstream to the substrate. This transport is both advective and conductive. The latter process results from electron-electron collisions which efficiently transfer energy between electrons confined to the magnetic field lines. In this respect one should expect that electrons which are heated in the ECR zone will remain fairly hot tens of cm downstream. One should also expect that excitation, dissociation, and ionization of the gas will occur in the vicinity of the substrate. This expectation has been confirmed by electric probe measurements of the electron temperature in ECR reactors which are discussed in Sec. II. Since the substrate is both bombarded by energetic particles, and may be immersed in a relatively hot plasma in which the feedstock gases are being excited and dissociated, the remote nature of ECR processing is problematic.

In this paper, we present results of a theoretical investigation of the electron energy distribution (EED) in ECR reactors as used for plasma processing of semiconductors. The goal of this work is to examine the transport of hot electrons from the ECR zone to regions near the substrate. This investigation has been conducted using a hybrid model which combines a Monte Carlo simulation (MCS), which generates details of the EED, with a simple fluid model which generates the ambipolar electric field. We find that the EED typically is not a Maxwellian even in the ECR zone and is often composed of two or more groups; a fairly low temperature component (a few eV) and a high energy tail which can extend for many 10s to 100s eV. The spatial distribution of the EED has two modes. At lower pressures (< 1 mTorr) the tail of the EED extends from the ECR region to the substrate (25 cm away). At pressures of a few mTorr and above, the tail of the EED is
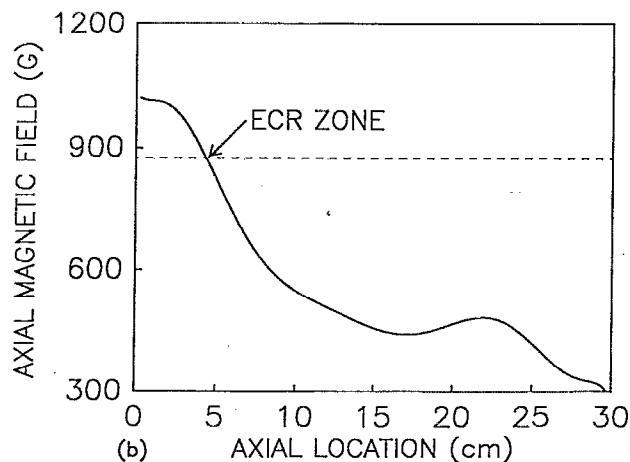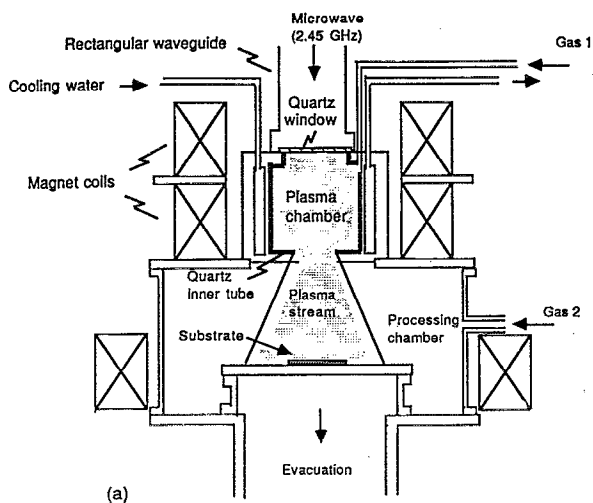

FIG. 1. (a) Schematic of a typical ECR reactor (see Ref. 16). This geometry was also used in this study. Magnetic field coils are used both upstream, to generate the ECR zone, and downstream to collimate the magnetic field. (b) Axial magnetic field profile used in this work. Three coils have been used to form a collimated B field.

depressed. These results are surprisingly not strong functions of the gas, at least for those discussed in this paper (Ar and N_2) and investigated elsewhere in our studies (O_2 and CF_4). This condition most likely results from the typically high plasma densities which increase the importance of electron-electron collisions compared to conventional rf diode discharges, and thereby mitigate differences in the EEDs which would otherwise occur.

In Sec. II, we will briefly review previous experimental measurements of the EED and electron temperature T_e for the ECR reactors of interest. The model is described in Sec. III, followed by a discussion of our results in Sec. IV. Our concluding remarks are in Sec. V.

II. SUMMARY OF MEASUREMENTS OF ELECTRON SWARM PROPERTIES IN ECR REACTORS

The configurations of ECR reactors being investigated for use in plasma processing are varied, and, so, the measurements of electron swarm properties are also varied.

The ECR reactor schematically shown in Fig. 1(a) is what we will call the standard configuration.[3,16] It consists of a cylindrical discharge region which expands to a larger diameter downstream where the substrate is placed. The magnetic field is typically supplied by one or more coils surrounding the ECR zone, with there being an optional coil downstream. The microwave field is propagated collinear to the axis of the reactor through a dielectric window. Using a coil downstream results in a magnetic field profile which is somewhat collimated; in the absence of that coil the magnetic field is flared.[3] A typical axial magnetic field, and the one used in this study, is shown in Fig. 1(b).

Variants of the standard configuration will place the substrate in or near the ECR zone[4] or use a rf bias on the substrate to increase or control the ion energies striking the substrate.[5,13] Alternate configurations use a tunable resonant cavity with a multicusp magnetic field configuration,[6] or an untuned cavity with a multipole magnetic field.[9] In the latter configurations, permanent magnets placed on the exterior of the chamber significantly reduce the loss of charged particles to the walls, and produce a uniform plasma. Unless otherwise noted, all experiments discussed below were performed at $v_r = 2.45$ GHz.

Measurements of the EED and electron temperature, T_e, in ECR discharges have been reported by a number of workers. (Use of the term T_e does not imply that the EED is a Maxwellian, but in the usual convention is defined as $T_e = \frac{2}{3}\langle \epsilon \rangle$, where $\langle \epsilon \rangle$ is the average electron energy.) Amemiya et al.[7] measured electron temperatures in N_2 and H_2 discharges in a cylindrical magnetic mirror device using a planar disk Langmuir probe located near the center of the mirror. They obtained temperatures of approximately 5 eV in N_2, and 9 eV in H_2 at 1 mTorr. These values increased with decreasing pressure to ≈ 12.5 eV and > 15 eV at 0.1 Torr for N_2 and H_2, respectively. They noted a depletion of the high energy tail of the distribution with respect to a Maxwellian at the same temperature, and a depletion of low energy electrons. The energy at which the distribution became depleted at high energy increased with decreasing gas pressure, and exceeded 100 eV at low pressures (<1 mTorr). Plasma densities were reported as approximately 10^{10} cm^{-3} for an input power of 100 W.

Amemiya and Ishii[8] performed similar measurements in a cylindrical multicusp ECR device (14 or 18 cm in diameter and 30 cm long) using a H_2/CH_4 gas mixture. At 0.6 mTorr ($H_2/CH_4 = 2.5/1$) the electron temperature was ≈ 16 eV at the ECR point, decreasing to ≈ 4 eV at a location 9 cm from the ECR zone. The plasma densities, $\approx 2 \times 10^{10}$ cm^{-3}, were nearly constant across the diameter of the device (20 cm) with a local maximum a few cm away from the ECR zone. Both T_e and the plasma densities in the ECR zone were nearly linear functions of incident power between 100 and 250 W. The EEDs were quite non-Maxwellian. The distribution near 10 eV was enhanced and a high energy tail extended to as much as 80 eV.

Hopwood et al.[6] also measured EEDs and plasma densities in a microwave tunable multipolar ECR reactor using Langmuir probes. At pressures of 0.1–10 mTorr in

argon, plasma densities were $3-10 \times 10^{11}$ cm^{-3} at micro-wave powers of 250 W. The plasma density decreased by a factor of nearly 5 in moving 10 cm downstream of the ECR zone. The average electron energy, though, was relatively constant over the same distance, at 5–7 eV. In fact, the electron temperature was itself fairly constant between 2 and 13 mTorr, increasing below 2 mTorr by about half at 0.5 mTorr. The measured EEDs were intermediate between a Maxwellian and a Druyvestyen near and downstream of the ECR zone. A high energy tail to the EED was not detected though the possibility of there being a tail in the ECR zone was not discounted. The absence of the high energy tail downstream may be caused by the local nature of the ECR zone and a depletion of the tail downstream, or a trapping of the high energy electrons in multipole magnetic cusps. The plasma potentials varied from 18 eV at high pressures (5–13 mTorr) to 28 eV at low pressure (0.5 Torr). The plasma potential decreased somewhat linearly below the ECR zone netting a steady state space charge field of 1.3 V cm^{-1}. That range of plasma potential has been confirmed by measurements of ion energy distributions.[10]

Electron temperatures were measured by Popov[11] in ECR plasmas sustained in N_2. Within the resonance region, or where the absorption of power from the microwave field occurred, the electron temperatures were 10–13 eV over a fairly large range of pressure (0.3 to 5 mTorr). Differences in electron temperature were predominantly found downstream of the ECR zone. In these cases, the electron temperature decreased to 3 eV at 5 mTorr and 10 cm downstream of the ECR zone, but decreased to only 8 eV for a pressure of 0.3 mTorr. The plasma potential at an intermediate pressure (0.6 mTorr) was approximately 25 V.

Electron temperatures in a variety of gases were measured using electric probes by Shirai et al.[12] Their measurements began approximately 15 cm downstream of the ECR zone. Electron temperatures in Ar were 2–6 eV for pressures of 6 to 0.2 mTorr. Similar measurements by Lee et al.[5] showed that the EED in the ECR zone of an Ar plasma (1 mTorr) has an average electron energy of 7 eV, and was intermediate between a Maxwellian and Druyvesteyn. They did not, though, detect a high energy tail to the EED.

Electron densities were measured by Pearton et al.[13] in a multipolar, tuned cavity ECR reactor in which the substrate could be biased using rf excitation. In a $CH_4/H_2/Ar = 5/17/8$ gas mixture (1 mTorr) the electron density was $1-2 \times 10^{11}$ cm^{-3} using only 10–50 W of rf excitation. The density was a factor of three larger using an additional 150 W of microwave excitation. Pure Ar plasmas (150 W microwave, 10 W rf) had electron densities of $1-2 \times 10^{11}$ for a gas pressure of 1 mTorr.

Carl et al.[17] measured ion densities and axial electric field profiles as a function of power deposition in a standard configuration. They found that the plasma operated in low mode and high mode configurations. In the low mode configuration at low powers ($<40-60$ W), the plasma densities in Ar were $<5 \times 10^{10}$ cm^{-3}, and the elec-

tric field penetrated downstream. In the high mode ($>40-60$ W) the ion densities increased linearly with power with values $>5 \times 10^{11}$ cm^{-3} at 100 W, and the field was nearly totally absorbed. In most cases, the maximum ion density occurred in the ECR zone.

The wide range of experimental results discussed here reflects the facts that the experimental apparatuses are themselves quite varied, and that the manner of power deposition critically depends on details of the magnetic field profile and electric field modes. One can, however, generalize to some extent. In the ECR systems of interest the electron temperature in the ECR zone at moderate power depositions (100–500 W) is 10–20 eV for argon. The electron temperature in the ECR zone increases with increasing power deposition and decreasing gas pressure (0.1 mTorr to a few mTorr), though not dramatically. The existence of a high energy tail to the EED in the ECR zone is generally accepted though not always measured. The electron temperature decreases downstream of the plasma zone in a manner which is more sensitive to gas pressure. Plasma potentials are in the range of 15–25 V, and generally increase with decreasing pressure and increasing power deposition. The dependence of plasma potential on these parameters is somewhat more sensitive than that for the electron temperature.

III. DESCRIPTION OF THE MODEL

The basis of our model for EEDs in ECR reactors is a previously published Monte Carlo simulation (MCS) of electron swarms which is capable of resolving electron-electron collisions in a time and spatially dependent manner.[18] This MCS is iteratively combined with a fluid model for charge densities in the ECR reactor to generate ambipolar electric fields. These fields are cycled back to the MCS and the procedure is iterated.

The geometry used in this investigation is a cylindrical ECR reactor [see Fig. 1(a)]. The magnetic field is supplied by a set of annular coils. The number and location of these coils can be specified in the model. The configuration used approximates a collimated magnetic field[3] [see Fig. 1(b)]. The length of the reactor in the model is 30 cm, a value somewhat shorter than standard reactors, but chosen to reduce the length of the calculations. It does, however, resemble the reactor of Carl et al.[17] The reactor is terminated by a dielectric window on one side and a floating substrate on the other. A circularly polarized electric field ($\nu_c = 2.45$ GHz) is incident from the left side of the cylinder and propagates along the axis of the cylinder with the electric field oriented perpendicular to the axis of the cylinder. The applied magnetic field is assumed to be azimuthally symmetric with the ECR point located approximately 5 cm from the dielectric window. The magnetic field at location $\mathbf{r} = (r,z)$ is simply given by the sum of the contributions of individual current loops in the coils,

$$\mathbf{B}(\mathbf{r}) = \sum_i \frac{\mu_o I_i}{4\pi} \int \frac{d\mathbf{l}_i \times (\mathbf{r} - \mathbf{l}_i)}{|\mathbf{r} - \mathbf{l}|^3} \qquad (1)$$

where I_i is the current carried by current loop i and l_i is its location. In practice, only the relative currents in the coils are specified. The desired location of the ECR point is selected and the absolute value of the currents in the coils are adjusted so that the axial magnetic field provides a resonance at that location. With an axial magnetic field having a "beach" configuration,[2] the resulting resonance surface resembles a shallow dome.

The microwave electric field as a function of position is handled fairly simply in the model with there being no attempt to predict any modal structure. We assumed that the electric field is a plane wave with uniform amplitude as a function of radial position in the reactor. The wave propagates collinear with the axis of the reactor so that the instantaneous electric field amplitude at any location is $E(z)\sin(\omega t - kz)$. We specified the amplitude of the incident electric field at the window and assumed that the subsequent amplitude of the electric field is totally determined by the exchange (either positive or negative) of energy with plasma electrons. To explicitly include both the resonant and nonresonant exchange of power between the electric field and the plasma electrons, the amplitude of the electric field is calculated from

$$\frac{1}{2\mu_0 c}\frac{dE^2(z)}{dz} = \sum_i N_i e \mathbf{E}(z)\cdot\mathbf{v}_i\delta(z_i - z), \qquad (2)$$

where the sum is over the electron pseudoparticles in the simulation, N_i is the number of electrons per unit volume that electron particle i represents, and $\mathbf{v}_i$ is its velocity.

The MCS simulation used in this work is derived from that described in detail in Ref. 18. The MCS explicitly includes electron-electron collisions by having the electron pseudoparticles collide with both the heavy particle fluid consisting of neutral and ionized atoms, and a velocity resolved electron fluid. The velocity distribution of the electron fluid as a function of position and time is forced to mirror that of the electron pseudoparticles by sampling the velocity distribution of the pseudoparticles on a regular basis and updating the distribution of the electron fluid. The MCS makes extensive use of a modified null cross section technique to account for changes in the electron density and electron velocity distribution as a function of position. This technique is also discussed in detail in Ref. 18.

The electron trajectories are explicitly integrated as a function of time in the MCS throughout the reactor using the local values of the electric and magnetic fields. Considering that the Larmor radius of electrons is $\simeq 100$ μm at a resonance and that the cyclotron frequency 2.45×10^9 s^{-1}, this approach is a considerable computational burden. We typically take time steps of $5 \times 10^{-12} \times$ to 1×10^{-11} s and use a third-order Runga–Kutta integration technique. This order of integration is sufficient to keep the error in energy to less than 1% over 10^3–10^4 periods. There are algorithms which can be used at resonance which treat the microwave electric field as a dc field, thereby allowing the integrating time step to be as large as the time between collision (a guiding center approximation). However during the time between collision ($\simeq 0.1$–0.2 μs) an electron with even a

moderate parallel component of velocity can move into or out of the resonance region. Given this condition, and the facts that both the magnetic and electric fields are functions of position and have multiple vector components, we chose not to modify these algorithms and to directly integrate the equations of motion of the pseudoparticles.

The plasma potential in the ECR reactors of interest is $10s$ V as shown by both electric probe measurements and measurements of ion energy distributions.[6,8,10] This results in an electrostatic space charge field of a few V cm^{-1}, which translates to an E/N of $100s$ to $1000s$ of Td (1 Td $= 10^{-17}$ V cm^2). The confining nature of an electric field having these values of E/N can significantly affect the spatial distribution of the electrons, and hence the spatial distribution of electron impact excitation and ionization of the feedstock gases. To obtain the space charge field, E_s, we constructed a simple fluid model for the ion and electron densities in which the continuity equations are solved under the assumption of ambipolar diffusion along the axis of the reactor. This model is admittedly an approximation because a fluid description for charge densities is poor at the low pressures of interest. The results of the model for the ambipolar potential, though, are in surprisingly good agreement with experiments, as discussed below. Recent results from a Monte Carlo simulation for ion transport in ECR reactors[19] have shown that ion motion is mobility limited at pressures of only a few mTorr, which may explain the success of our fluid model.

In the fluid model, we solve the continuity equations for electrons and ions along the axial dimension of the ECR reactor in the steady state

$$\frac{\partial n}{\partial t} = \sum_i n_e k_I^i N_i + \nabla\cdot(D_L\nabla n \pm n\mu E_s) - \frac{D_T n}{\Lambda^2} = 0, \qquad (3)$$

where n is either the ion or electron density, n_e is the electron density, k_I^i is the rate coefficient for electron impact ionization of neutral species i, D_L is the longitudinal diffusion coefficient, μ is the mobility, D_T is the transverse diffusion coefficient, and Λ is the diffusion length in the radial direction. The ionization rate coefficients and electron transport coefficients are obtained from the MCS as a function of axial position but are averaged over the radius of the discharge. The continuity equations are solved using a matrix inversion technique. In the case of argon, its metastable states are included in the model.

Since the plasma density exceeds 10^{10} cm^{-3} for most cases of interest, transport in the axial direction will be ambipolar limited in the bulk of the plasma. E_s can therefore be obtained from

$$E_s = \frac{D_L^-\nabla_L n_e - D_L^+\nabla_L n_I}{\mu_e n_e + \mu_I n_I}, \qquad (4)$$

where the subscripts L, e, and I denote the longitudinal value, electrons, and ions, respectively. After completion of the fluid model, the longitudinal space charge field is cycled back to the MCS and included in the equations of motion for the electrons. This iterative procedure between the MCS and fluid model is typically repeated four times. Electron particles are added and subtracted from the sim-
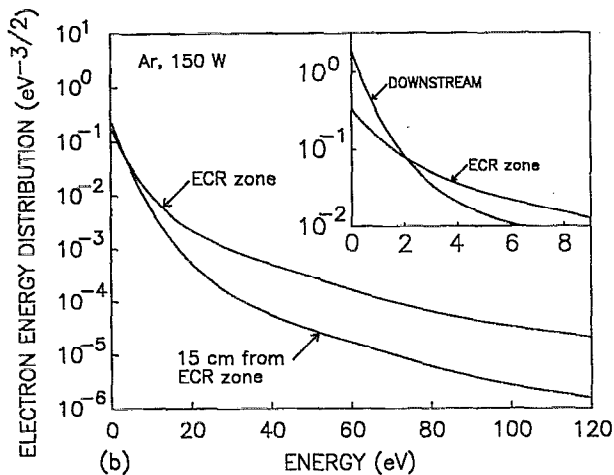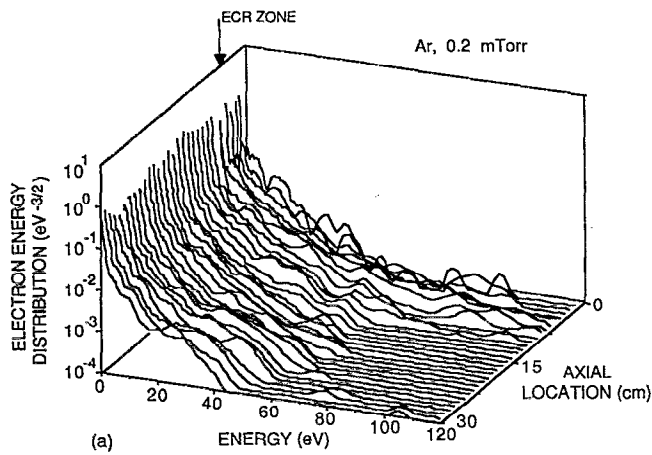
(a)

(b)

FIG. 2. Simulated electron energy distributions (EEDs) in Ar plasmas (0.2 mTorr, 150 W). (a) EED as a function of position showing the lifting of the EED in the ECR zone. (b) EED in the ECR zone and 15 cm downstream. These latter EEDs have been smoothed using a polynomial fit. The inset shows a more accurate representation of the lower portion of the EEDs. The lower portion of the EED cools faster than the tail which persists downstream.

(a)

(b)

FIG. 3. Predicted electron temperatures in ECR Ar plasmas (150 W). (a) T_e as a function of axial location. (b) T_e vs pressure. The experimental curve was taken from Ref. 6 for similar conditions. The electron temperature increases with decreasing pressure, approaching 20 eV in the ECR zone at pressures < 1 mTorr.

ulation as ionizations and losses occur. One indication of convergence is that the net rate of change in the number of electron particles is nearly zero.

IV. ELECTRON SWARM PARAMETERS IN ECR REACTORS

In this section we will present results from our model for electron swarm parameters in ECR reactors. Unless otherwise noted, the ECR reactor is cylindrical with coaxial magnetic field coils as described in Sec. II. The length of the reactor is 30 cm and the diameter is 14 cm. The ECR point is chosen to occur at approximately 5 cm. A schematic of the reactor and the axial magnetic field as a function of position are shown in Fig. 1.

A. Argon plasmas

The EED as a function of position in an Ar plasma (0.2 mTorr, 150 W) is shown in Fig. 2(a). The EED in the ECR zone and 15 cm downstream of the ECR zone are separately shown in Fig. 2(b). The electron temperature as
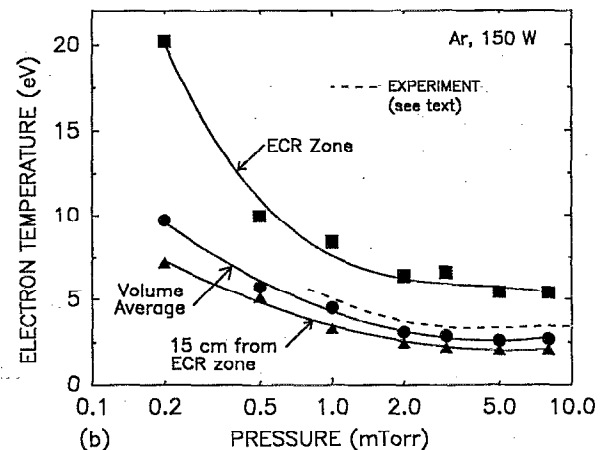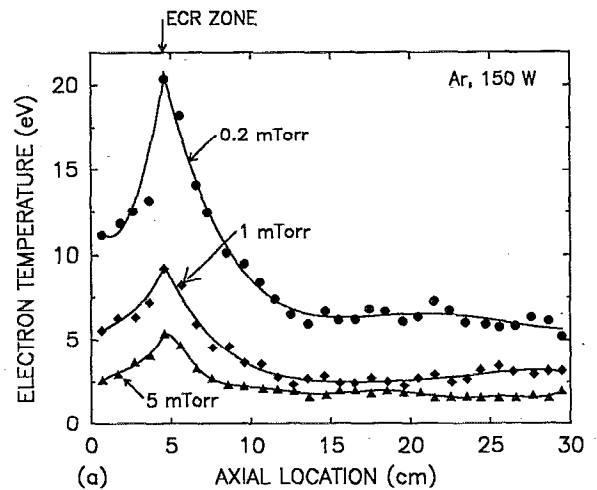
a function of position and Ar pressure is shown in Fig. 3. The reactor averaged electron density is $\approx 2 \times 10^{10}$ cm^{-3} for these conditions. The density increases with increasing pressure. At 1 mTorr, the density is $\approx 4 \times 10^{11}$ cm^{-3}, which corresponds to the high mode operation of Carl et al.[17] The EED is not well described by a Maxwellian, and varies significantly between the ECR zone and downstream. In the ECR zone, where power is dominantly channeled into the electron swarm, the tail of the EED is raised at the expense of the lower energy portion of the distribution, and extends beyond 120 eV. The EED in the ECR zone can be described by at least two temperatures, 5–7 eV for energies of < 15 eV and 15–20 eV for energies > 20 eV. The distribution averaged temperature, 12–13 eV, is more characteristic of the higher energy group. The EED 15 cm downstream of the ECR zone differs from that in the ECR zone in that the lower portion of the distribution has cooled to 2.5–3.5 eV, a consequence of inelastic collisions and drift against the axial ambipolar electric

field. The higher energy portion of the distribution, however, can still be characterized by a temperature of 15–20 eV. Its density, though, is smaller by more than an order of magnitude. The persistence of the high energy portion of the EED is a consequence of the lower collision frequency for electrons having energies greater than 10s eV. The ambipolar potential for these conditions is $\approx$40 V. The cutoff in the distribution at approximately 40 eV is partly a consequence of higher energy electrons being able to escape the plasma.

The electron temperature is relatively constant as a function of position outside the ECR zone, decreasing moderately from a "plateau" value acquired outside the ECR zone.[6] The electron swarm takes 5–10 cm to reach its plateau value from its peak in the ECR zone. The electron temperature increases with decreasing gas pressure, from 2–3 eV far downstream at pressures of many mTorr, to 15–20 eV in the ECR zone at pressures < 1 mTorr. The change in T_e is moderate above 1 mTorr and increases more dramatically below 1 mTorr. The dashed line in Fig. 3(b) shows measurements from Hopwood et al.[6] for similar conditions, showing the trend of increasing T_e at pressures below a few mTorr. The predicted values of T_e downstream of the ECR zone also agree well with the measurements of Shirai et al.[12] as a function of pressure and microwave power.

During the time that 30 eV electrons which have half their energy in the perpendicular component move 5–10 cm out of the ECR zone, they experience 5–10 collisions, of which 15%–20% are inelastic. The decrease in T_e observed in the first 5–10 cm outside of the ECR zone is likely a consequence of electrons with moderate energies above the inelastic thresholds (12–40 eV) having a few inelastic collisions which decrease their energy to below the inelastic thresholds. Once this happens, the energy loss is dominantly by elastic collisions, which proceeds at a far slower rate. The high energy tail, which has commensurately lower collision frequencies, takes longer to have these few collisions and therefore persists for a longer time (or distance). Its lower rate of energy exchanging e-e collisions makes the tail less sensitive to thermalization than the lower portion of the EED. The loss of higher energy electrons which climb the plasma potential and escape from the reactor ultimately determines the energy at which the distribution is cut off.

At energies of less than a few eV [see inset to Fig. 2(b)] the EED appears to have an anomalously high thermal component, similar to that seen in some radio frequency (rf) discharges,[20] though most likely resulting from a different mechanism. The low energy component is weak in the ECR zone, and increases outside the ECR zone. This feature is characteristic of microwave discharges sustained in argon in which the momentum transfer collision frequency, ν_m, is much less than the oscillation frequency (radians) of the electric field, ω. Ferreira et al.[21,22] attributes this effect to the fact that power transfer is maximum in nonmagnetized plasmas at the energy at which $\nu_m(\epsilon) = \omega$, and since $\nu_m(\epsilon)$ increases with increasing energy up to 20–30 eV, the tail of the distribution is
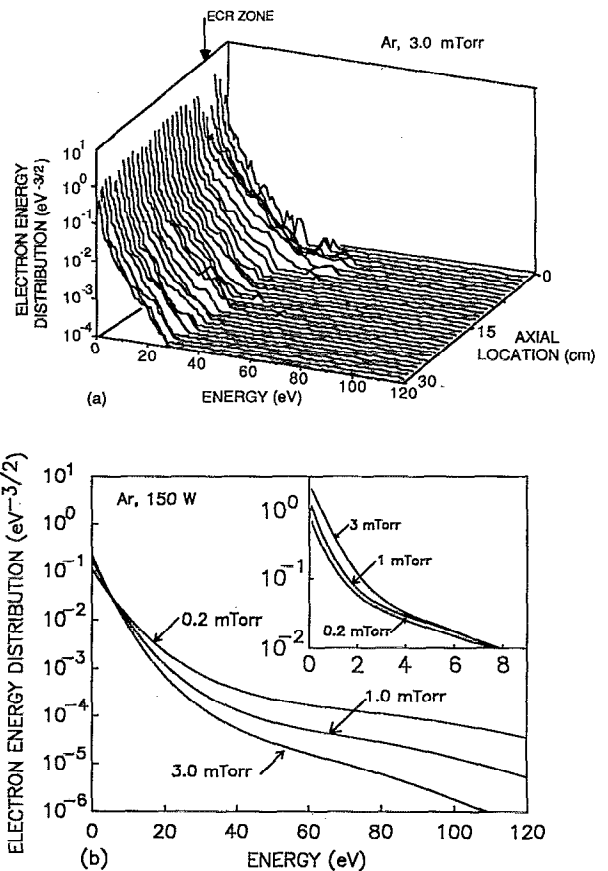

FIG. 4. Electron energy distributions as a function of pressures. (a) EED as a function of position for a 3 mTorr Ar plasma. (b) Reactor averaged EEDs for pressures of 0.2, 1, and 3 mTorr. These latter EEDs have been smoothed using a polynomial fit. More accurate representations of the lower portion of the EED are shown in the inset.

enhanced at the expense of the lower energy electrons. Since power transfer does not critically depend on $\nu_m(\epsilon)/\omega$ in the ECR zone, as excitation appears quasi-dc, the discrimination between the low energy and high energy components is less severe. This effect should therefore not be important in the ECR zone. Outside the ECR zone, the nonresonant interaction between the electric field and the gyrating electrons prevents significant power transfer. The enhancement of the very low portion of the distribution is then dominantly due to inelastic collisions.

The EED as a function of position for a 3 mTorr discharge in Ar is shown in Fig. 4(a), plotted on the same scale as Fig. 2(a) for comparison. EEDs for 0.2, 1, and 3 mTorr, averaged over the ECR reactor, are shown in Fig. 4(b). The EED in the ECR zone has a less pronounced high energy tail at 3 mTorr, compared to 0.2 mTorr. The tail is also depleted downstream by collisions at a more rapid rate compared to the lower pressure. This depletion of the tail of the EED at higher pressure is similar to the effect observed by Amemiya et al.[7] and discussed in Sec. II. All of these observations are consistent with simply having a lower effective value of E/N when operating at fixed microwave power and increasing the gas pressure.[12] The
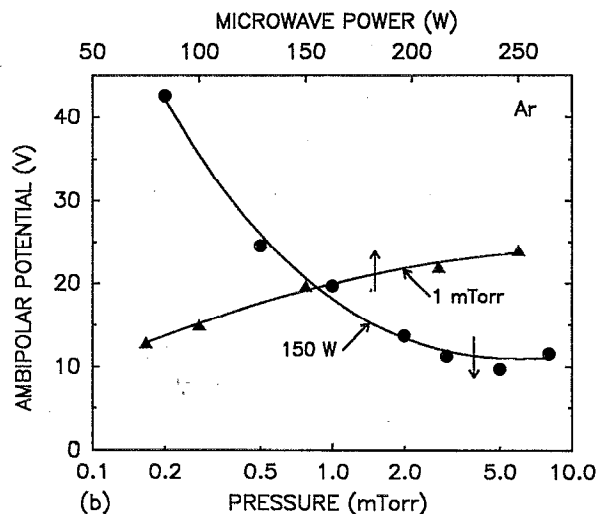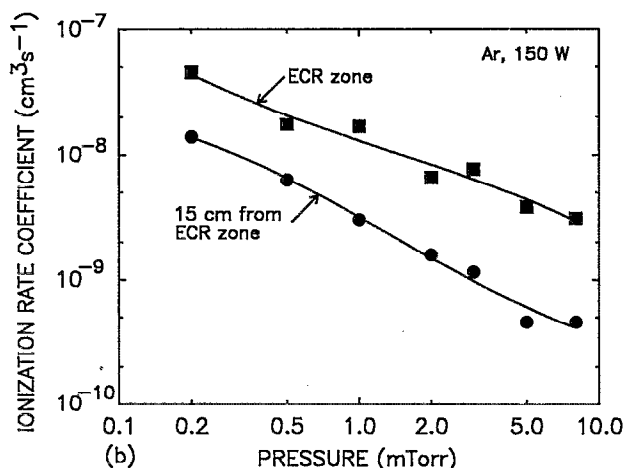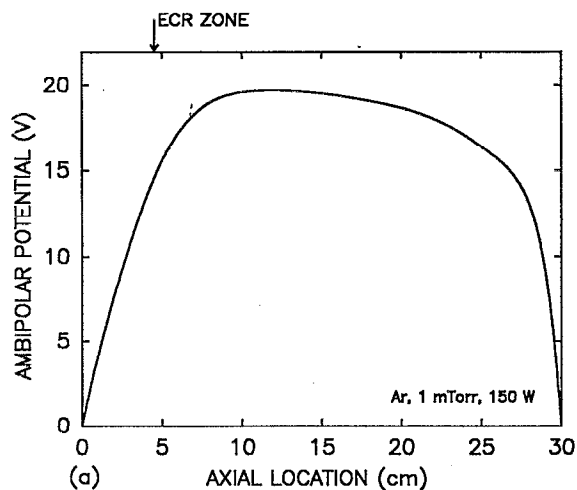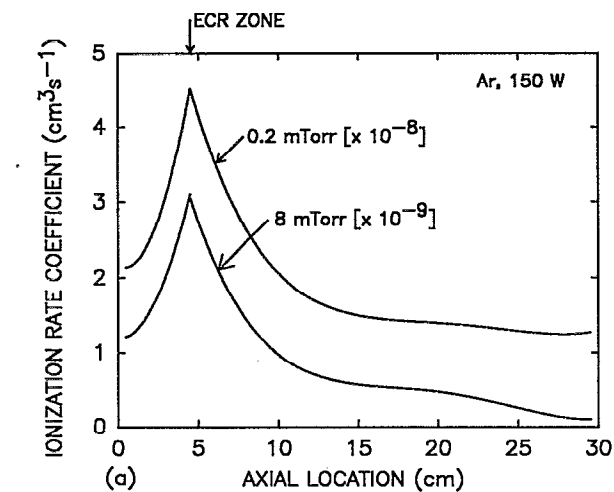
Y. Weng and M. J. Kushner   38

FIG. 5. Ionization rate coefficients in Ar (150 W) as a function of (a) position (smoothed) and (b) pressure. These coefficients decrease by only a factor of 3–5 downstream at low pressure compared to their values in the ECR zone resulting in substantial ionization downstream. Ionization rate coefficients decrease with increasing operating pressure commensurate with operating at a lower effective E/N.

FIG. 6. Ambipolar potential in Ar plasmas as a function of (a) position (150 W), and (b) pressure and microwave power. The maximum potential is displaced towards the ECR zone from the center of the reactor due to the maximum in ionization being displaced in a similar manner. The maximum potential increases moderately with increasing microwave power. At pressure <1 mTorr, the potential increases to many 10s V.

lower energies at which the EED is cut off at higher pressures is also a consequence of a lowering of the ambipolar potential which allows lower energy electrons to escape from the plasma (see below).

The distribution averaged rate coefficients for ionization of ground state Ar are shown in Fig. 5 as a function of axial location and pressure. The shape of the rate coefficients closely follow the electron temperature though their magnitude decreases more severely with pressure than does the electron temperature. At pressures of less than a few mTorr, the rate coefficients downstream remain commensurate with those in the ECR zone, decreasing by only a factor of 3. This indicates that a substantial amount of ionization occurs adjacent to remotely mounted substrates. The disparity in ionization rates between the ECR zone and downstream increases with increasing pressure, a consequence of a higher rate of inelastic energy losses at the higher pressures.

The statistics of this method are poor at high electron energies as shown by the noise in the distributions. The excitation rates are most sensitive to the noisiest portion of the distribution. Much of the noise in the distribution is hidden by the fact that quoted temperatures and rate coefficients are moments over the distribution which tends to smooth the noise. The scatter in rate coefficients is at worst 10%, as shown in Fig. 5(b).

Predictions for the ambipolar potential as a function of position, gas pressure, and microwave power appear in Fig. 6. The ambipolar potential increases with increasing gas pressure, moderately above 1 mTorr and more rapidly below 1 mTorr, in agreement with experiments.[6] The ambipolar potential increases with increasing microwave power, also in agreement with experiment. The increase in the ambipolar potential is commensurate with the increase in electron temperature with increasing microwave power as shown in Fig. 7. In our model, the ambipolar potential is determined by electron transport along the axis parallel to the magnetic field. The reduction in electron mobility
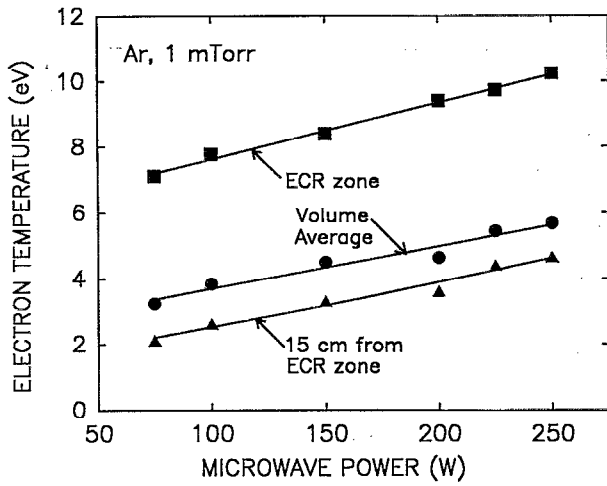
FIG. 7. Electron temperature in Ar plasmas (1 mTorr) as a function of microwave power. T_e increases moderately with power, causing a moderate increase in ambipolar potential.
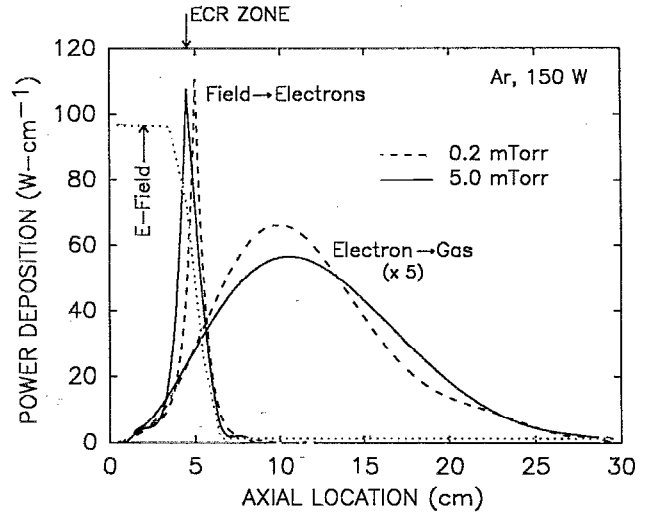

FIG. 8. Power deposition as a function of position in Ar plasmas (150 W) at 0.2 and 5 mTorr. Power transfer from the field to electrons ($f \rightarrow e$) and electrons to the gas ($e \rightarrow g$) are shown, as well as the amplitude of the microwave electric field for the 5.0 mTorr case. Power transfer to the gas is displaced from the ECR zone towards the maximum in the ambipolar potential and electron density. This effect may be exaggerated here.

transverse to the magnetic field (in our radial direction) implies that the ambipolar electric field in that direction should be small, and makes a correspondingly small contribution to the total ambipolar potential. These features have, in fact, been seen in the results of the 2-d simulations of Porteous and Graves for ECR discharges.[23] The predicted maximum in the ambipolar potential is not in the ECR zone but is displaced towards the center of the reactor. For otherwise constant conditions, the higher electron temperature in the ECR zone should result in higher rates of ionization, a larger ambipolar electric field, and a maximum in the ambipolar potential at that location. The displacement of the maximum in the ambipolar potential out of the ECR zone is a consequence of our model predicting a maximum in the total rate of ionization outside the plasma zone. This situation will be discussed further below. Our results predict a somewhat higher ambipolar potential at low pressures (<1 mTorr) than may be experimentally observed. This may result from our use of a fluid model to obtain the ambipolar field which underpredicts the ion drift velocity for a given E/N, and therefore results in a larger ambipolar electric field to compensate.

Power deposition in unmagnetized microwave gas discharges is given by[24]

$$P(z) = e^2 n_e \overline{E}^2(z)/(m_e \nu_m), \quad \overline{E}^2 = E^2 \frac{\nu_m^2}{\nu_m^2 + \omega^2}, \quad (5)$$

where n_e and m_e are the electron density and mass, ν_m is the momentum transfer collision frequency, and ω is the microwave (radian) frequency. $\overline{E}$ is an effective electric field and E is the actual electric field. In the limit that $\omega \gg \nu_m$, there is little net power transfer to either the electrons or the gas since the electrons simply oscillate 90° out of phase with the alternating electric field. Collisions are, in fact, required for a time averaged net transfer of power to the gas. Under conditions of ECR excitation (which is spatially uniform) the effective electric field becomes

$$\overline{E}^2 = \frac{E^2}{2} \frac{\nu_m^2}{\nu_m^2 + (\omega - \omega_c)^2}. \quad (6)$$

The effective width of the resonance zone increases with increasing gas pressure due to an increase in ν_m. Although these formulas are, in general accurate, they do not give a fair representation of power deposition in ECR reactors since power is transferred to the electron swarm in a fairly localized region while electrons are highly mobile along the magnetic field lines.

Excitation and ionization in gas discharges actually occur in two steps. The first is transfer of power from the electric field to the electron swarm, denoted here as $f \rightarrow e$. The second is transfer of power from the electrons to the gas by collisions, denoted here as $e \rightarrow g$. In higher pressure discharges, $f \rightarrow e$ and $e \rightarrow g$ power transfers occur in the same spatial location and the expressions in Eqs. (5) and (6) are valid. In low pressure ECR reactors where in the absence of Doppler effects the width of the ECR zone may be thin compared to the mean free path of electrons, the locations of power transfer by $f \rightarrow e$ and $e \rightarrow g$ processes may be quite different. For example, the collision frequency for inelastic energy loss for a 50 eV electron in Ar at 1 mTorr is 7×10^6 s^{-1}. In our geometry, the grad-B force points downstream out of the ECR zone. Assuming that the particle energy is primarily in the perpendicular component, an electron travels about 5–10 cm before having a collision. This distance is long compared to the width of the ECR zone (a few mm to a few cm when considering Doppler effects).

The spatial distributions of power deposition for $f \rightarrow e$ and $e \rightarrow g$ processes in Ar at 0.2 and 5.0 mTorr are shown in Fig. 8. Power deposition for $f \rightarrow e$ logically occurs dominantly of the ECR zone. In our model, oscillations in the

$f \rightarrow e$ power deposition downstream of the ECR zone occur from the statistical scatter of the Monte Carlo method in which power is exchanged positively and negatively between the electrons and the microwave field. These oscillations have been smoothed for these profiles but typically are not more than a few percent of the maximum. The width of the $f \rightarrow e$ power deposition results dominantly from the shallow domelike structure of the ECR surface since the full width of the ECR zone corresponds to only a few Gauss in the absence of Doppler effects. Power transfer by $f \rightarrow e$ occurs somewhat closer to the dielectric window at 5 mTorr since the width of the region in which efficient power deposition occurs is wider at the higher pressure, and the plasma density is higher. The amplitude of the electric field, shown for 5 mTorr in Fig. 8, decreases to near zero in traversing the ECR zone, though there is some penetration in our model. This corresponds to the high mode operation observed by Carl et al.[17] When we modeled lower power deposition (< 50–75 W) cases, significantly more field penetration occurred with corresponding decrease in plasma density which resembles the low mode configuration of Carl et al. We cannot, however, resolve any true model behavior of the electric field with this model.

The power deposition for $e \rightarrow g$ occurs dominantly outside the ECR zone where the maximum in the electron density predicted by the fluid model occurs. The ambipolar potential restricts the axial loss of electrons and displaces the maximum of the electron density away from the ECR zone. The persistence of large rate coefficients for inelastic energy loss downstream of the ECR zone results in a substantial amount of $e \rightarrow g$ power transfer at those locations.

The shift between the $f \rightarrow e$ and $e \rightarrow g$ power deposition is most likely over estimated and is a weakness of the hybrid particle-fluid techniques used here. For example, Carl et al.[17] measures a maximum in the ion density and presumably ion production rate in the ECR zone. The tendency of our fluid model is to average the effects of the transport coefficients of the low- and high-temperature portions of the EED. The more populous low energy electrons, which have lower mobilities, determine the ambipolar potential. The fluid model then attempts to place the maximum of the plasma potential and density near the center of the reactor. Rate coefficients obtained from the particle simulation, generated by the high-temperature electrons are therefore weighted by distribution average densities to too great a degree towards the center of the plasma. So, in spite of higher rate coefficients for ionization in the ECR zone, the higher total rate of ionization is predicted outside the zone. The more accurate method is to transfer source functions, instead of rate coefficients, from the Monte Carlo simulation to the fluid model. This method would more closely align the maximum in both $f \rightarrow e$ land $e \rightarrow g$ of power transfer near the ECR zone. This method was subsequently used in a hybrid model for radio frequency discharges.[25]

The power dissipation in the Ar plasma is dominantly shared between electron impact ionization and ion acceleration. At 2 mTorr and 150 W, 0.21 of the power is dis-
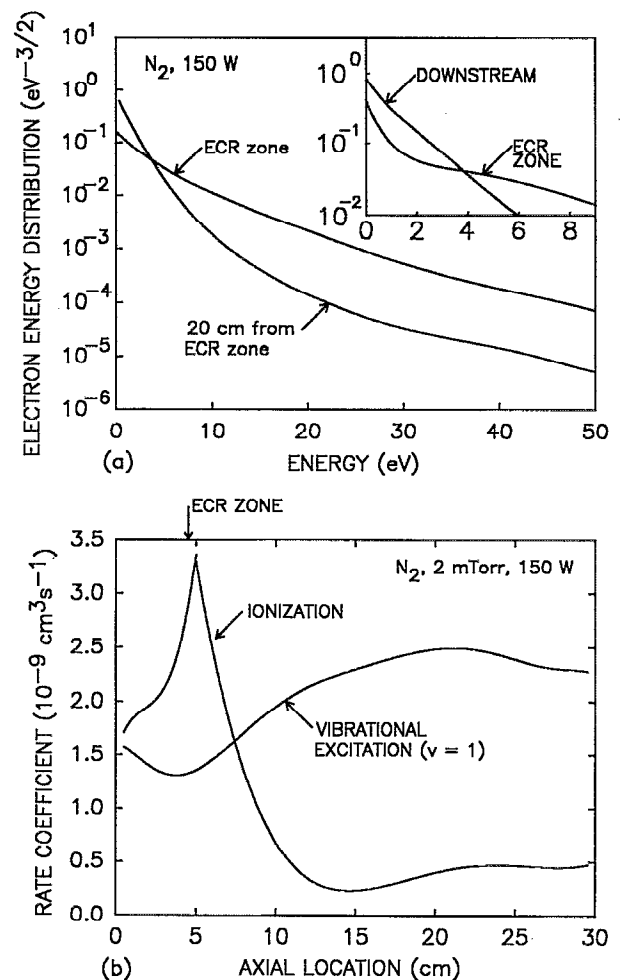

FIG. 9. Electron swarm parameters in N_2 ECR plasmas (2 mTorr, 150 W). (a) EEDs (smoothed using a polynomial fit) in the ECR zone and downstream. More accurate representations of the EEDs at low energy are shown in the inset. (b) Rate coefficients (smoothed) for ionization and vibrational excitation. The rate coefficients for vibrational excitation are depressed in the ECR zone due to depletion of the low energy portion of the EED.

sipated by electronic excitation, 0.36 by electron impact ionization, and 0.43 by ion acceleration. Since the ion mean free path for charge exchange is < 2 cm at 2 mTorr, approximately 0.3–0.4 of the power dissipated by ion acceleration goes into gas heating, and the remainder goes into substrate heating. As the pressure decreases, the fraction of power dissipated by ion acceleration increases. At 0.2 mTorr, ≈ 0.67 of the power is dissipated by ion acceleration.

B. N_2 plasmas

EEDs in the ECR zone and 15 cm downstream for N_2 plasmas are shown in Fig. 9(a). The qualitative features of these EEDs are similar to those in Ar. The average electron energies are 13.9 and 3.8 eV, respectively, commensurate with those measured by Popov.[11] The anomalous low energy component of the EED, typically found in Ar plasmas, is not as pronounced in the N_2 plasmas.

The rate coefficients for ionization and vibrational excitation of ground state N_2 are shown in Fig. 9(b) as a function of axial location. The ionization rate coefficient has a similar shape to that for argon, having a maximum in the ECR zone and decreasing outside the ECR zone. The rate coefficient for vibrational excitation, though, has the opposite dependence. This is a consequence of vibrational excitation resulting from collisions of low energy electrons ($\epsilon \leqslant 4$ eV) while ionization results from collisions with higher energy electrons ($\epsilon \geqslant 15$ eV). Heating of the EED in the ECR zone results in a depletion of the lower energy portion of the EED. This causes a depression in the rate coefficient for vibrational excitation and an increase in the rate coefficient for ionization. As the distribution cools outside the ECR zone, the rate coefficient for vibrational excitation rebounds, while that for ionization decreases.

The transport coefficients described here were obtained only using cross sections for N_2 whereas in the experimental device a significant amount of dissociation may occur. The average amount of dissociation can be estimated from conservation equations for N_2 and N.

$$\frac{dN_2}{dt}=\frac{[N_2]_o-N_2}{\tau}-n_e\sum_i k_{di}N_2+\frac{D_N s}{2\Lambda^2}=0, \qquad (7a)$$

$$\frac{dN}{dt}=\frac{-N}{\tau}-\frac{D_N Ns}{\Lambda^2}+2n_e\sum_i k_{di}N_2=0. \qquad (7b)$$

In Eq. (7), τ is the average residence time of gas in the reactor, $[N_2]_o$ is the input density, k_{di} is the rate coefficient for electron impact dissociation by process i, D_N is the effective diffusion coefficient for N, and Λ is the transverse diffusion coefficient. s is the reactive sticking coefficient for $2N\rightarrow N_2$ on the walls of the reactor. Estimating $s=0.01$, and using values from the simulation for a pressure of 2 mTorr and 150 W, we obtain $N_2/[N_2]_o\approx0.8$–0.9. The N_2 is therefore moderately dissociated. An analysis performed at higher power depositions should include the consequences of dissociation on the electron transport coefficients.

The power balance in N_2 plasmas differs somewhat from Ar plasmas in that a smaller fraction of the power is dissipated by ionization. For example, at 2 mTorr and 150 W, the fractional power dissipation is 0.06 vibrational excitation, 0.49 electronic excitation, 0.09 dissociation, and 0.18 ionization, and 0.18 ion acceleration. Approximately 0.3–0.4 of the power dissipated by ion acceleration goes into gas heating.

V. CONCLUDING REMARKS

A model for the electron energy distribution in ECR reactors for plasma processing has been constructed and results presented for discharges in Ar and N_2. The electron temperature in Ar varies from a few eV downstream of the ECR zone at pressures of many mTorr, to almost 20 eV in the ECR zone at pressures of less than 1 mTorr. The maximum ambipolar potential for these conditions varies from 10–15 V to 40 V. The bulk electron temperature decreases downstream of the ECR zone fairly rapidly. The high energy tail of the EED persists farther downstream. These effects, and the disparity in $f\rightarrow e$ and $e\rightarrow g$ power transfer,

result in ionization rate coefficients in both Ar and N_2 remaining relatively high downstream compared to their values in the ECR zone. A substantial amount of ionization and excitation occurs adjacent to the substrate in ECR reactors in spite of $f\rightarrow e$ power transfer occurring remotely from the substrate.

[1] D. L. Flamm and G. K. Herb, in *Plasma Etching: An Introduction*, edited by D. M. Manos and D. L. Flamm (Academic, Boston, 1989) pp. 1–90, and references therein.
[2] J. Asmussen, J. Vac. Sci. Technol. 7, 883 (1989).
[3] W. M. Holber and J. Forster, J. Vac. Sci. Technol. A 8, 3720 (1990).
[4] S. Samukawa, S. Mori, and M. Sasaki, J. Vac. Sci. Technol. A 9, 85 (1991).
[5] Y. H. Lee, J. E. Heidenreich, and G. Fortuno, J. Vac. Sci. Technol. A 7, 903 (1989).
[6] J. Hopwood, K. K. Reinhard, and J. Asmussen, J. Vac. Sci. Technol. A 8, 3103 (1990).
[7] H. Amemiya, K. Shimizu, S. Kato, and Y. Sakamoto, Jpn. J. Appl. Phys. 27, L927 (1988).
[8] H. Amemiya and S. Ishii, Jpn. J. Appl. Phys. 28, 2289 (1989).
[9] T. D. Mantei and S. Dhole, J. Vac. Sci. Technol. B 9, 26 (1991).
[10] W. M. Holber and J. Forster, J. Vac. Sci. Technol. 8, 3720 (1990).
[11] O. A. Popov, J. Vac. Sci. Technol. A 7, 894 (1989).
[12] K. Shirai, T. Iizuka, and S. Gonda, Jpn. J. Appl. Phys. 28, 897 (1989).
[13] S. J. Pearton, T. Nakano, and R. A. Gottscho, J. Appl. Phys. 69, 4206 (1991).
[14] T. Nakano, N. Sadeghi, and R. A. Gottscho, Appl. Phys. Lett. 58, 459 (1991).
[15] E. A. Den Hartog, H. Persin, and R. Claude Woods, Appl. Phys. Lett. 57, 661 (1990).
[16] S. Matsuo and M. Kinchu, Jpn. J. Appl. Phys. 22, L210 (1983).
[17] D. A. Carl, M. C. Williamson, M. A. Lieberman, and A. J. Lichtenberg, J. Vac. Sci. Technol. B 9, 339 (1991).
[18] Y. Weng and M. J. Kushner, Phys. Rev. A 42, 6191 (1990).
[19] M. A. Hussein and G. A. Emmert, J. Vac. Sci. Technol. A 8, 2913 (1990).
[20] V. A. Godyak and R. B. Piejak, Phys. Rev. Lett. 65, 996 (1990).
[21] C. M. Ferreira, "Theory of high-frequency discharges," in *Nonequilibrium Processes in Partially Ionized Gases*, edited by M. Capitelli and J. N. Bardsley (Plenum, New York, 1990), pp. 187–212.
[22] C. M. Ferreira, L. L. Alves, M. Pinheiro, and A. B. Sa, IEEE Trans. Plasma Sci. 19, 229 (1991).
[23] R. K. Porteous and D. B. Graves, IEEE Trans. Plasma Sci. 19, 204 (1991).
[24] S. C. Brown, *Basic Data of Plasma Physics* (Wiley, New York, 1959).
[25] T. J. Sommerer and M. J. Kushner, J. Appl. Phys. 71, 1654 (1992).